

Oxidation Response of Transpiration Cooled ZrB_2 on a Hypersonic Stagnation Point

Marc Ewenz Rocher ^{*}, Tobias Hermann [†] and Matthew McGilvray [‡]

*The University of Oxford, Department of Engineering, Osney Mead, The Southwell Building,
Oxford OX2 0ES, United Kingdom*

This work presents the oxidation response of a transpiration cooled hypersonic stagnation point made of porous ZrB_2 . Low order models are used to calculate the surface temperature and oxygen concentration for a given flight condition. An analytical material oxidation model computes the surface recession and oxide layer thickness. A 500 s steady state trajectory at 44 km altitude and 3.6 km/s velocity is found to lead to 2.2 mm recession of the 3 mm nose radius. A constant mass injection at a blowing parameter of 0.6 reduces the recession to just 0.21 mm. The displacement of freestream oxygen by transpiration cooling has a significant effect on oxidation. Not accounting for the displacement of oxygen at the surface would increase the recession by up to 197%. The recession along the transient trajectory of an envisioned hypersonic vehicle with a 3 mm nose radius is found to exceed 0.94 mm with no mass injection. It is shown that nitrogen and helium injection at a blowing parameter of 0.6 can reduce the recession to 0.13 mm and 0.075 mm, respectively.

Nomenclature

B_h	=	heat blowing parameter
B_m	=	mass blowing parameter
B^*	=	boundary layer blowoff parameter
C	=	concentration, mol/m ³
c	=	mass fraction
c_p	=	specific heat capacity, J/kg K
$D_{i,j}$	=	binary diffusion coefficient for species i and j
F	=	blowing ratio
Fn	=	function of
f	=	porosity of oxide scale

^{*}DPhil Candidate, Oxford Thermofluids Institute, University of Oxford, AIAA Member.

[†]Departmental Lecturer, Oxford Thermofluids Institute, University of Oxford, AIAA Member.

[‡]Associate Professor, Oxford Thermofluids Institute, University of Oxford, AIAA Member.

k	=	thermal conductivity, W/m K
h	=	specific enthalpy, J/kg
h_D	=	average dissociation enthalpy, J/kg
h_{ext}	=	thickness of external boria layer, m
h_{int}	=	thickness of internal boria layer, m
h_v	=	volumetric heat transfer coefficient, W/m ³ K
$ J $	=	diffusive flux, mol/m ² s
K_m	=	mass transfer coefficient, m/s
L	=	scale thickness, m
L_1	=	sample thickness, m
Le	=	Lewis number
M	=	molar mass, g/mol
N_f	=	atomic correction factor
\dot{n}	=	formation rate, mol/m ² s
Pr	=	Prandtl number
p	=	pressure, Pa
p_{O_2}	=	oxygen partial pressure, Pa
\dot{q}	=	heat flux, W/m ²
r	=	nose radius, m
R	=	surface recession, m
Sc	=	Schmidt number
St_h	=	$\frac{\dot{q}}{\rho u (h_e - h_w)}$, Stanton number for heat transfer
St_m	=	$\frac{K_m}{u}$, Stanton number for mass transfer
T	=	temperature, K
t	=	time, s
u	=	velocity, m/s
x	=	distance along the surface, m
y	=	mole fraction
z	=	distance normal to the surface, m
Δ	=	shock stand-off distance, m
ε	=	emissivity
λ	=	scaling factor

μ	=	viscosity, Pa s
$\Pi_{\text{O}_2-\text{B}_2\text{O}_3}$	=	oxygen permeability in liquid boria, m ² /s
ρ	=	density, kg/m ³
σ	=	Stefan-Boltzmann constant
τ	=	empirical correction factor
ϕ	=	porosity

Subscripts

0	=	no blowing
cold	=	cold wall
cond	=	conductive
e	=	boundary layer edge
ext	=	external gas
film	=	coolant film
fluid	=	fluid
inj	=	injected gas
int,adv	=	internal advective
pl	=	plenum
rad	=	radiative
reduced	=	reduced
s	=	solid
w	=	wall
∞	=	freestream gas

Superscripts

a	=	ambient
i	=	liquid vapor interface
s	=	substrate
zb	=	zirconia boria interface

I. Introduction

HYPERSONIC flight is characterized by extreme aerodynamic heating. This results in elevated surface temperatures and chemical reactions, such as oxidation and nitration. The most exposed vehicle components are the stagnation points, both for blunt and slender vehicles [1]. As they generally pose the most stringent limit to the flight envelope,

thermally and chemically protecting them is critical. For slender vehicles, an additional requirement for the leading edges is shape-stability, thereby excluding the use of ablatives. High melting temperature aerospace materials such as UHTCs [2–4] or C/C composites [5, 6] reduce the incident, hot wall corrected convective heat flux, while drastically increasing passive cooling through re-radiation. This passive cooling potential, however, remains untapped due to the early onset of oxidation at temperatures below 1000 K [7]. It is therefore highly desirable to mitigate the surface oxidation of hypersonic stagnation points.

Transpiration cooling is a potential means to reduce oxidation [8]. This active thermal protection system feeds a fluid through a porous wall, cooling it through internal convection. Upon exiting, the coolant forms a protective film that reduces part of the aerothermal heating [9] and catalytic heating [10]. Additionally, the film reduces the mole fraction of freestream oxygen at the surface [11].

Oxidation depends on both the temperature and oxygen partial pressure at the wall [7]. Thus, transpiration cooling has two mitigating effects on oxidation: it lowers the surface temperature and reduces the oxygen partial pressure by displacing the freestream oxygen with an oxygen-free injectant. In the existing literature, the oxidation response of a hypersonic stagnation point has only been investigated experimentally for no blowing [12]. The oxidation protection provided to any material by transpiration cooling has not been dealt with, despite its significance in enabling higher operating temperatures and thus extending the hypersonic flight envelope.

In this paper, the oxidation response of transpiration cooled ZrB_2 on a hypersonic stagnation point is modeled. This is achieved by combining three analytical models for heat transfer, oxygen concentration and the ZrB_2 oxidation response. The combined model is then applied to three increasingly complex test cases: A furnace with constant temperature and pressure and no transpiration cooling, a steady state flight path with blowing and a transient flight path with blowing.

II. Model Overview

This section outlines the working principles and assumptions of the models used in this work. A schematic of the work flow is provided in Fig. 1. The analysis starts with an initial guess for the surface temperature, and by defining the trajectory of the vehicle. The resulting post-shock gas properties, together with the emissivity, nose radius, coolant type and amount of blowing, are fed into the heat transfer model.

By balancing the heat fluxes acting on the model, illustrated in Fig. 2, an updated surface temperature is found. This process is repeated until the temperature converges. Below 800 K, no oxidation will occur. The maximum operating temperature of ZrB_2 , before it starts softening is assumed to be 3000 K, given that the melting point is at 3519 K. Within this range, the oxygen partial pressure at the surface is computed, before it is fed into the oxidation model. The oxidation kinetics of ZrB_2 depend on the thickness of the boria layer, as illustrated in Fig. 5. The appropriate oxidation model is chosen and outputs three oxidation parameters: the oxide scale thickness, the boria layer depth and the surface recession.

This is the first model predicting the oxidation behavior of transpiration cooled ZrB_2 on a hypersonic stagnation

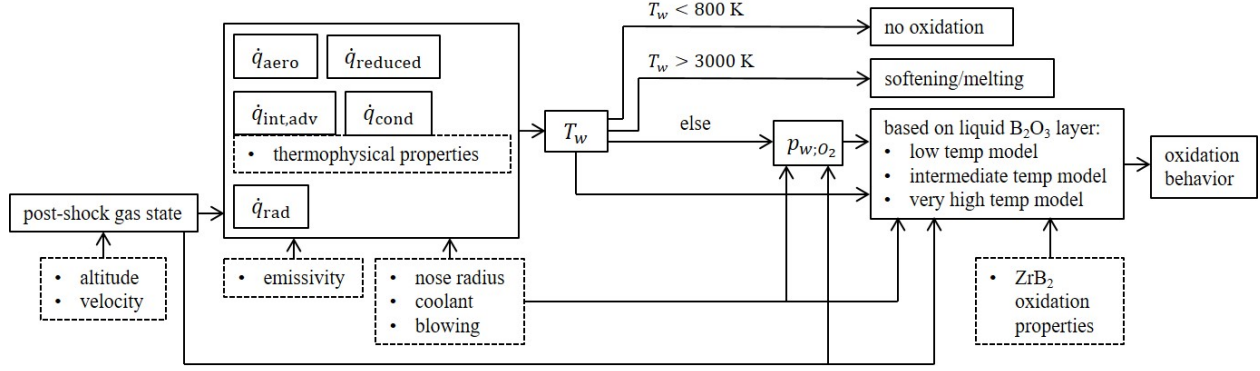


Fig. 1 Flow chart of the numerical approach.

point. Due to the lack of existing literature, the following simplifying assumptions were made:

- 1) the flow is in thermochemical equilibrium.
- 2) atomic oxygen causes the same oxidation behavior as molecular oxygen.
- 3) the substrate porosity does not affect the oxidation rate.
- 4) mass injection does not change the aerodynamic radius.

In the following, the models are described more extensively.

A. Heat transfer model

It is possible to conduct a full CFD simulation for every condition along the flight trajectory. However, time and computational cost make this very impractical. Instead, the approach used here employs established correlations and simplified numerical models to compute the surface temperature of a transpiration cooled hypersonic stagnation point by balancing the heat fluxes on a 1-D porous wall with mass injection, as shown in Fig. 2. Note that due to the 1-D assumption, lateral heat fluxes were ignored. The backside of the porous material is assumed to be adiabatic, as the conductivity of the coolant is low and the radiated heat will mostly be reflected back by the sub-structure [13].

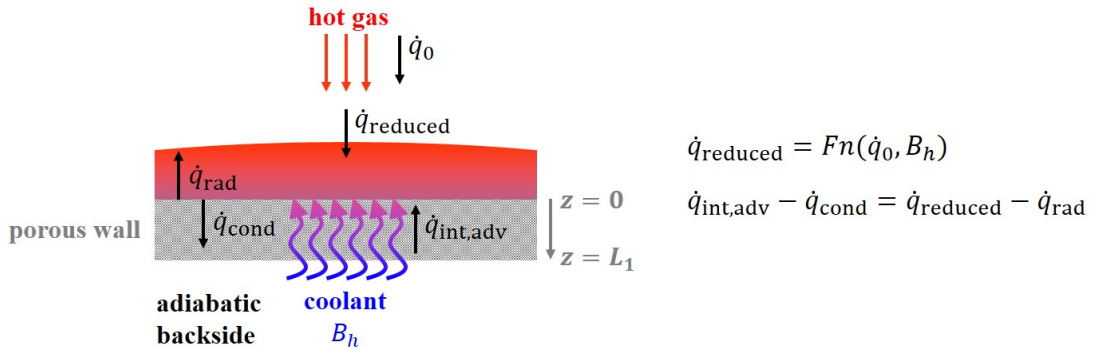


Fig. 2 Heat balance on a 1-D stagnation point.

The convective aerodynamic heat transfer for a hypersonic stagnation point in the absence of mass injection is

calculated by the Fay-Riddell [14] correlation:

$$\dot{q}_0 = 0.76 Pr_w^{-0.6} (\rho_w \mu_w)^{0.1} (\rho_e \mu_e)^{0.4} \left(1 + \left(Le^{0.52} - 1 \right) \frac{h_D}{h_e} \right) (h_e - h_w) \sqrt{\frac{du_e}{dx}}, \quad (1)$$

where the Prandtl and Lewis number are assumed to be $Pr = 0.71$ and $Le = 1.4$, respectively. The heat flux reduction due to mass injection is commonly described using the non-dimensional heat blowing parameter

$$B_h = \frac{F}{St_{h0}} \quad (2)$$

where the blowing ratio, F , and uncooled Stanton number, St_{h0} , are defined as

$$F = \frac{\rho_{inj} u_{inj}}{\rho_{\infty} u_{\infty}} \quad (3)$$

$$St_{h0} = \frac{\dot{q}_0}{\rho_{\infty} u_{\infty} (h_e - h_w)}. \quad (4)$$

The heat flux reduction due to blowing is computed using the correlation presented in Ref. [15]

$$\frac{St_h}{St_{h0}} = \frac{\dot{q}_{\text{reduced}}}{\dot{q}_0} = \frac{1}{\sqrt{K}} \frac{e^{\frac{-1}{\pi} K B_h^2}}{1 + \text{erf} \left(\sqrt{\frac{1}{\pi} K} \right) B_h} \quad (5)$$

$$K = \frac{\Delta}{\Delta_0} \tau^{\frac{B_h}{B^*}} \quad (6)$$

where B^* is defined as

$$B^* = 1.59 \sqrt{\frac{M_{inj}}{M_{\infty}}} \quad (7)$$

Throughout this study, the chosen blowing parameters, B_h were smaller than the boundary layer blowoff parameter, B^* .

The shock stand-off ratio is calculated as follows:

$$\frac{\Delta}{\Delta_0} = 1 + \sqrt{\frac{\rho_s}{\rho_{\infty}} \frac{M_{\infty}}{M_{inj}}} St_{h,0} B_h \quad (8)$$

Finally, the empirical correction factor τ accounts for the molecular weight of the injected fluid as follows:

$$\tau = \sqrt{\frac{M_{\infty}}{M_{inj}}} N_f \quad (9)$$

with $N_f = 5/9$ for monatomic and $N_f = 1$ for polyatomic gases. Figure 3 shows the relationship between the heat

blowing parameter and the Stanton number reduction for the parameters in Table 1, encountered by a 3 mm nose radius at 44 km altitude and 3.6 km/s velocity, cooled by nitrogen and helium injection.

Table 1 Parameters used in Fig. 3

M_∞	M_{inj}	St_{h0}	ρ_∞	ρ_s
[g/mol]	[g/mol]	[-]	[kg/m ³]	[kg/m ³]
28.97	28 (N ₂) , 4 (He)	0.14	0.0022	0.0233

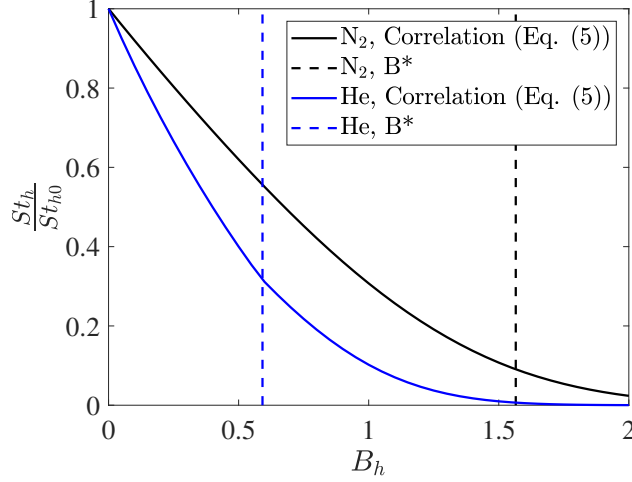


Fig. 3 Stanton number reduction due to blowing, indicating blowoff parameter.

The wall temperature is obtained by balancing the reduced aerodynamic heat flux, $\dot{q}_{reduced}$, with re-radiation, \dot{q}_{rad} , internal advective cooling, $\dot{q}_{int,adv}$ and conduction \dot{q}_{cond} . This can be achieved by simultaneously solving the steady-state energy equations of the fluid and solid in the porous medium, given as

$$\underbrace{\rho_f u_f c_{p,f} \frac{dT_f}{dz}}_{\text{internal advection}} = \underbrace{h_v (T_s - T_f)}_{\text{fluid-solid heat exchange}} \quad (10)$$

$$\underbrace{k_s (1 - \phi) \frac{dT_s^2}{dz^2}}_{\text{conduction}} = \underbrace{h_v (T_f - T_s)}_{\text{solid-fluid heat exchange}} \quad (11)$$

Eq. (10) balances the advective heat flux of the transpiring fluid with the fluid-solid heat exchange, while Eq. (11) equals the conductive heat flux through the solid with the solid-fluid heat exchange. These coupled ordinary differential equations are solved analytically [16] and the following boundary conditions are applied:

$$T_f|_{z=L_1} = T_{pl} \quad (12)$$

$$\left. \frac{dT_s}{dz} \right|_{z=L_1} = 0 \quad (13)$$

where T_{pl} is the coolant temperature in the plenum and the second boundary condition denotes the adiabatic backside. The net incident heat flux is applied at the front surface:

$$k_s (1 - \phi) \left. \frac{dT_s}{dz} \right|_{z=0} = \dot{q}_{\text{reduced}} - \dot{q}_{\text{rad}} \quad (14)$$

where the radiative heat flux is obtained from the Stefan-Boltzmann law

$$\dot{q}_{\text{rad}} = \varepsilon \sigma T_s^4|_{z=0}. \quad (15)$$

Note that $z = L_1$ denotes the cooled side and $z = 0$ the heated side.

B. Oxygen concentration model

The oxygen concentration on a hemispherical transpiration cooled hypersonic stagnation point can be obtained for any freestream condition, nose radius and injection parameters, using the correlation developed in Ref. [17]. It requires knowledge of the viscosity, density and velocity gradient at the boundary layer edge, as well as the Schmidt number and the mass flux at the wall, all of which are readily available. If the injected gas differs from the freestream gas, an additional correction for the molar mass and diffusion coefficient is required. The mass fraction of air at the wall is then found as follows:

$$c_{\text{air},w} = \frac{St_m}{St_{m0}} = \frac{\lambda B_m}{e^{\lambda B_m} - 1} \quad (16)$$

using the mass blowing parameter B_m with a scaling factor λ from Ref. [17], which are defined as follows:

$$B_m = \frac{F}{St_{m0}} \quad (17)$$

$$St_{m0} = 0.89 \frac{\rho_e}{\rho_w} \frac{\mu_e}{\sqrt{\rho_w \mu_w}} \sqrt{\frac{\partial u_e}{\partial x}} \frac{1}{u_e} \quad (18)$$

$$\lambda = \left(\frac{\mu_e T_w}{\mu_w T_e} \right)^{0.5} Sc_w^{0.6} 2.52 \frac{\rho_e}{\rho_w} \times \left(\frac{M_{\text{ext}} D_{\text{ext-ext}}}{M D_{\text{inj-ext}}} \right)_w^{0.75} \quad (19)$$

All high temperature quantities, in particular the molar mass of dissociated air are obtained using the CEA-NASA code [18]. The diffusion coefficients are calculated using kinetic theory with the Lennard-Jones parameters [19]. Figure 4

visualizes the relationship between the scaled blowing parameter and the mass Stanton number ratio.

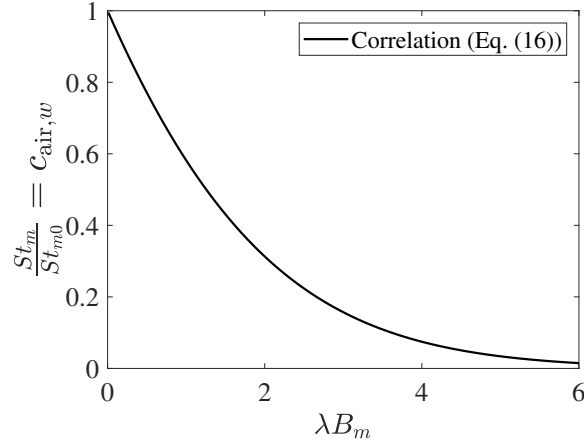


Fig. 4 Relationship between the mass blowing parameter and the Stanton number ratio.

The oxygen partial pressure at the wall is found as follows:

$$y_{\text{air},w} = \frac{c_{\text{air},w}/M_{\text{air}}}{c_{\text{air},w}/M_{\text{air}} + (1 - c_{\text{air},w})/M_{\text{inj}}} \quad (20)$$

$$y_{\text{O}_2,w} = 0.21 y_{\text{air},w} \quad (21)$$

$$p_{\text{O}_2,w} = p_e y_{\text{O}_2,w} \quad (22)$$

The edge pressure, p_e is obtained from normal shock relations for a given freestream condition. Note that the pressure field around the stagnation point is not affected by injection when the blowing parameter is smaller than the boundary layer blowoff parameter, $B_h < B^*$.

From the

C. Oxidation model

The analytical oxidation model applied in this work was developed by Parthasarathy et al. [20]. When ZrB_2 oxidizes, it produces a porous ZrO_2 scale, as well as liquid or gaseous B_2O_3 , depending on the temperature and oxygen pressure [7], as shown in Fig. 5. The analytical model quantifies the diffusion of oxygen through the oxide scale and the boron layer and assumes it to be the rate limiting step for oxidation activity at the substrate.

The model was developed for dense ZrB_2 , but as no porous ZrB_2 oxidation model is available in the existing literature, it was deemed suitable for this initial study. Figure 6 shows the cross-section of a 42% porous ZrB_2 substrate,

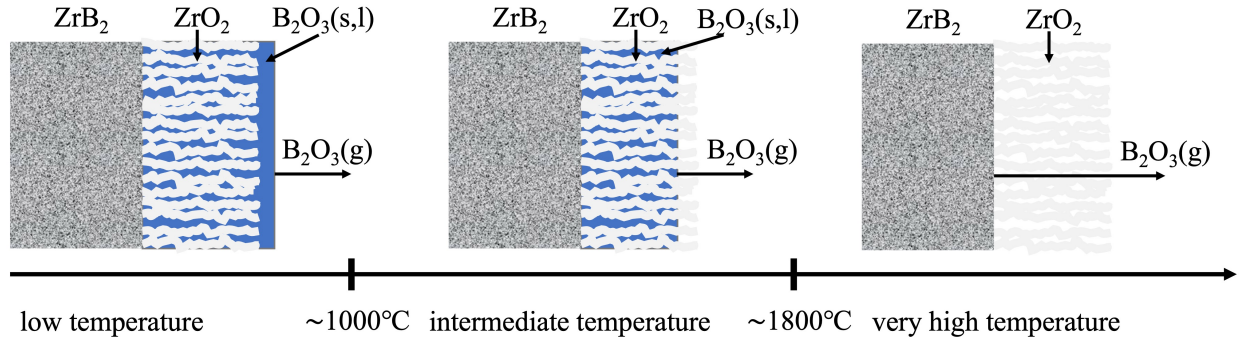


Fig. 5 Oxidation regimes of ZrB₂ [7].

which was heated to 2150 K in a plasma wind tunnel [8]. The ZrO₂ scale has the same columnar microstructure as in Fig. 5. The 42% porosity of the substrate therefore did not affect the oxidation microstructure, encouraging the use of the aforementioned oxidation model for porous substrates.

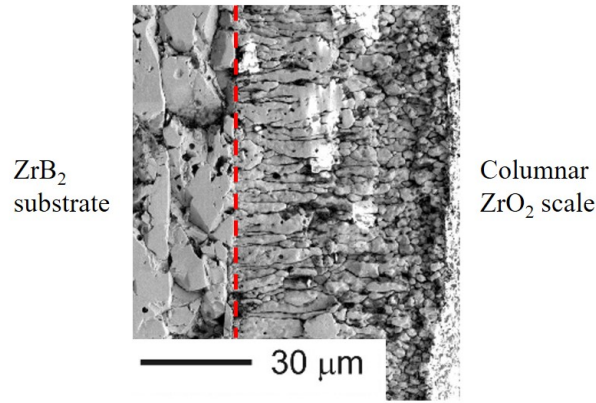
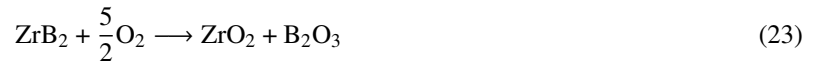


Fig. 6 Cross-section of porous ZrB₂ after an exposure time of 60 seconds at 2150 K [8]

The model presented in this work only predicts the oxidation behavior on the surface of the porous interface, marked by the dotted line in Fig. 7, as the diffusion into a porous medium against a pressure gradient has not yet been modeled quantitatively in the existing literature. This diffusion is strongly dependent on the material microstructure. By not accounting for the adverse pressure gradient, the model will overpredict oxidation for the blowing cases [11]. It thus provides a conservative estimate of the oxidation protection provided by mass injection. The uncooled cases do not have a pressure gradient and are therefore not affected by this simplification.

In all temperature regimes shown in Fig. 5, the following reaction takes place at the ZrB₂ surface



If atomic oxygen is present, it is assumed that it recombines and behaves the same as molecular oxygen. Therefore, the

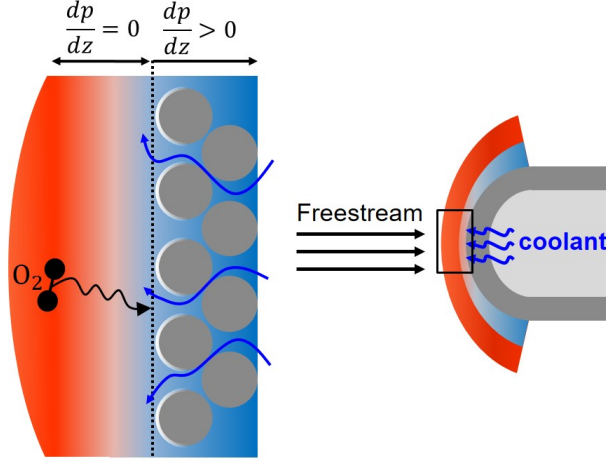


Fig. 7 Schematic of oxidation of porous interface, adapted from Ref. [11].

rate of formation of zirconia, \dot{n}_{ZrO_2} , is proportional to the rate of oxygen diffusion to the substrate.

$$\dot{n}_{\text{ZrO}_2} = \frac{2}{5} |J_{\text{O}_2}| \quad (24)$$

Taking into account the porosity of the oxide scale, $f = 0.05$, the scale thickness growth is obtained as

$$\begin{aligned} \frac{dL}{dt} &= \left(\frac{M_{\text{ZrO}_2}}{\rho_{\text{ZrO}_2}} \right) \left(\frac{1}{1-f} \right) \dot{n}_{\text{ZrO}_2} \\ &= \left(\frac{M_{\text{ZrO}_2}}{\rho_{\text{ZrO}_2}} \right) \left(\frac{1}{1-f} \right) \frac{2}{5} |J_{\text{O}_2}| \end{aligned} \quad (25)$$

Following the numerical integration of Eq. (25), the magnitude of recession of the ZrB_2 substrate is given by

$$R = L (1-f) \frac{M_{\text{ZrB}_2} / \rho_{\text{ZrB}_2}}{M_{\text{ZrO}_2} / \rho_{\text{ZrO}_2}} \quad (26)$$

It remains to find the magnitude of oxygen diffusion through the ZrO_2 scale and the B_2O_3 layer to the ZrB_2 surface, $|J_{\text{O}_2}|$. The diffusion will be governed by a different mechanism for each of the three temperature regions of the oxidation model.

In the low temperature region, typically starting at around 600°C , the boria layer exceeds the thickness of the zirconia scale, as shown in Fig. 5. Oxygen must diffuse through the external boria layer and then through the pore channels up until the surface. In steady state, the oxygen flux through both regions must be equal, therefore

$$|J_{O_2}| = f \frac{\Pi_{O_2-B_2O_3}}{L} (p_{O_2}^{zb} - p_{O_2}^s) \quad (27)$$

$$= \frac{\Pi_{O_2-B_2O_3}}{h_{\text{ext}}} (p_{O_2}^a - p_{O_2}^{zb}) \quad (28)$$

where the temperature dependent correlations for $p_{O_2}^s$ and $\Pi_{O_2-B_2O_3}$ are provided by Eq. (10) and (12) of Ref. [7], respectively. The thickness of the external boria layer, h_{ext} , is found by balancing the rate of formation of liquid boria at the substrate, less that which resides in the porous scale and the rate of evaporation, using Eqs. (4) - (6) in Ref. [20]. Here, $p_{O_2}^a$ is the oxygen pressure at the ambient interface, which needs to be supplied by the oxidation model presented in section II.B. The ambient interface is equivalent to the wall and thus $p_{O_2}^a = p_{O_2,w}$ can be obtained from Eq. (22). $p_{O_2}^{zb}$ is found by equating Eqs. (27) and (28). Eq. (27) is then inserted into Eq. (25) to find the scale thickness and consequently the recession using Eq. (26).

At temperatures exceeding about 1000°C, the external layer evaporates and only a fraction of the scale length is filled with boria. In this intermediate regime, gaseous oxygen must diffuse through the pore channels and then permeate through the liquid boria layer at the end of the channel to reach the surface and react with virgin ZrB_2 . The rate of oxygen diffusion through the pores is given as

$$|J_{O_2}| = f D_{O_2} \frac{C_{O_2}^a - C_{O_2}^i}{L - h_{\text{int}}} \quad (29)$$

Here, $C_{O_2}^a$ is the concentration of oxygen at the scale-ambient interface, which needs to be supplied by the oxidation model presented in section II.B. The concentration of molecular oxygen at the boria liquid-vapor interface, $C_{O_2}^i$ is obtained by balancing the diffusion of boria through the oxide scale, $|J_{B_2O_3}|$ with the formation of boria at the ZrB_2 interface, $\dot{n}_{B_2O_3}$. The formation of boria is linked to the diffusion of oxygen via Eq. (23).

$$\dot{n}_{B_2O_3} = |J_{B_2O_3}| = f D_{B_2O_3} \frac{C_{B_2O_3}^i - C_{B_2O_3}^a}{L - h_{\text{int}}} = \frac{2}{5} |J_{O_2}| \quad (30)$$

and thus,

$$C_{O_2}^i = C_{O_2}^a - \frac{5}{2} \frac{D_{B_2O_3}}{D_{O_2}} (C_{B_2O_3}^i - C_{B_2O_3}^a) \quad (31)$$

where $C_{B_2O_3}^a$ is assumed to be zero and $C_{B_2O_3}^i$ is found from a temperature dependent correlation [7]. The last unknown variable in Eq. (29) is the boria layer thickness, h . It is found by balancing the diffusion of oxygen through the liquid

boria layer with its diffusion through the oxide scale.

$$|J_{O_2}(B_2O_3)| = |J_{O_2}| \quad (32)$$

$$f\Pi_{O_2-B_2O_3} \frac{P_{O_2}^i - P_{O_2}^s}{h} = fD_{O_2} \frac{C_{O_2}^a - C_{O_2}^i}{L - h_{int}}. \quad (33)$$

where $\Pi_{O_2-B_2O_3}$ and $P_{O_2}^s$ are found from a correlations [7] and $P_{O_2}^i = RTC_{O_2}^i$. Inserting Eq. (29) into (25) yields the scale thickness.

At elevated temperatures, the boria layer will evaporate completely. The oxidation will be limited by the rate of diffusion through the porous ZrO_2 scale [20]. The flux of oxygen and boria, as well as the balance of fluxes is given by

$$|J_{O_2}| = fD_{O_2} \frac{C_{O_2}^a - C_{O_2}^s}{L} \quad (34)$$

$$|J_{B_2O_3}| = fD_{B_2O_3} \frac{C_{B_2O_3}^a - C_{B_2O_3}^s}{L} \quad (35)$$

$$|J_{O_2}| = \frac{5}{2}|J_{B_2O_3}| \quad (36)$$

The boria concentration is assumed to be negligible at the ambient interface, $C_{B_2O_3}^a = 0$, and can be related to the oxygen concentration at the substrate, $C_{B_2O_3}^s = F(C_{O_2}^s)$, using Eq. (9) in Ref. [20]. Combining Eqs. (34) - (36), $C_{O_2}^s$ is found and inserted into Eq. (34). Further increasing the temperature to about 2500°C leads to evaporation of the oxide layer, thereby accelerating oxidation and surface recession. Eq. (25) is amended to account for this as follows

$$\left(\frac{M_{ZrO_2}}{\rho_{ZrO_2}}\right) \left(\frac{1}{1-f}\right) \frac{2}{5} |J_{O_2}| - J_{evap;ZrO_2} \quad (37)$$

where $J_{evap;ZrO_2}$ is found from a correlation provided in Eq. (15) of [20].

A more detailed derivation of the model equations used in this study can be found in Refs. [7] and [20]. With this model one can calculate the scale thickness, virgin surface recession and boria layer thickness for a given temperature and oxygen partial pressure.

III. Results and Discussion

Three cases are examined in this study, schematically depicted in Fig. 8. In the first, the oxidation behavior of a ZrB_2 substrate with no mass injection is investigated. The second case studies the oxidation behavior of a transpiration cooled stagnation point on a steady state trajectory. Finally, a transient trajectory of an envisaged hypersonic vehicle is examined. Table 2 shows the thermophysical properties of the ZrB_2 substrate modeled in this work.

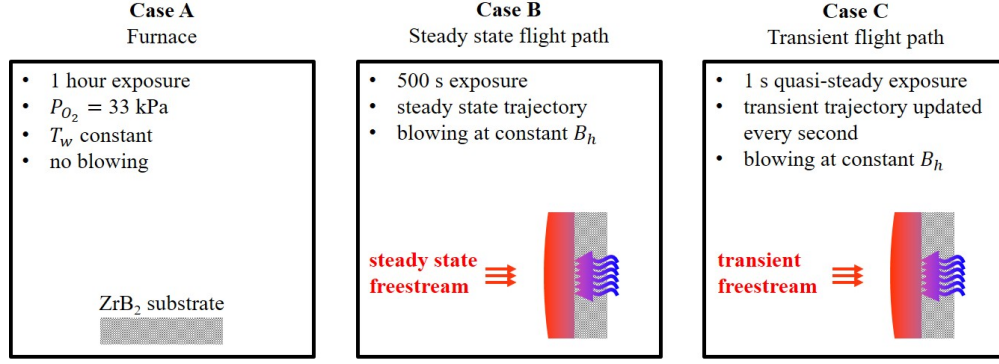


Fig. 8 Illustration of the three cases examined in this study.

Table 2 Coolant temperature and material properties [2] used in this study.

T_{pl}	ε	h_v	L_1	ϕ	k_s
[K]	[-]	[W/m ³ K]	[mm]	[-]	[W/mK]
300	0.7	5.5×10^4	2.5	0.42	41.4

Case A: Oxidation behavior with no mass injection

In this case the ZrB₂ substrate is placed in the furnace for 1 hour at constant temperature and 33 kPa of pure oxygen. Fig. 9 shows the oxide scale thickness, recession and boria layer depth as a function of time for a fixed temperature of 1500 K.

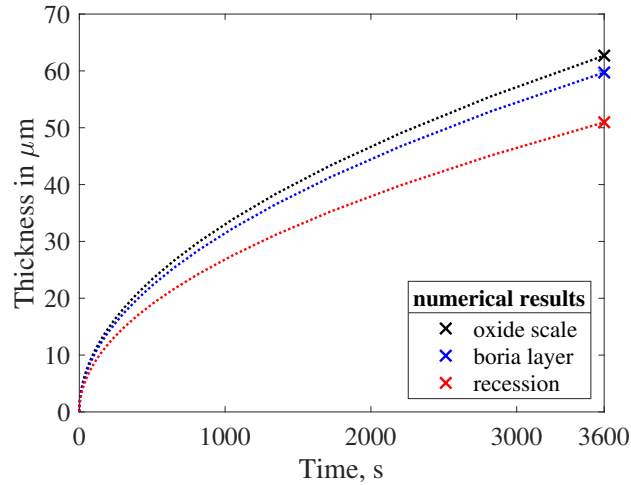


Fig. 9 Oxide scale, recession and boria layer growth over time at 1500 K and 33 kPa of pure oxygen.

The oxidation rate decelerates as the oxide layer grows and shields the substrate with the mechanisms detailed in section II.C. The markers indicate the final thickness of all three quantities after an exposure time of 1 hour. This calculation was then repeated for temperatures between 800 K and 2800 K. The final values, denoted by the markers were plotted against temperature in Fig. 10. All data points in this figure were obtained numerically. The numerical implementation

of the code in this work was validated against Fig. 4 of Ref. [20], which also modeled the oxidation after a 1 hour exposure at 33 kPa of pure oxygen.

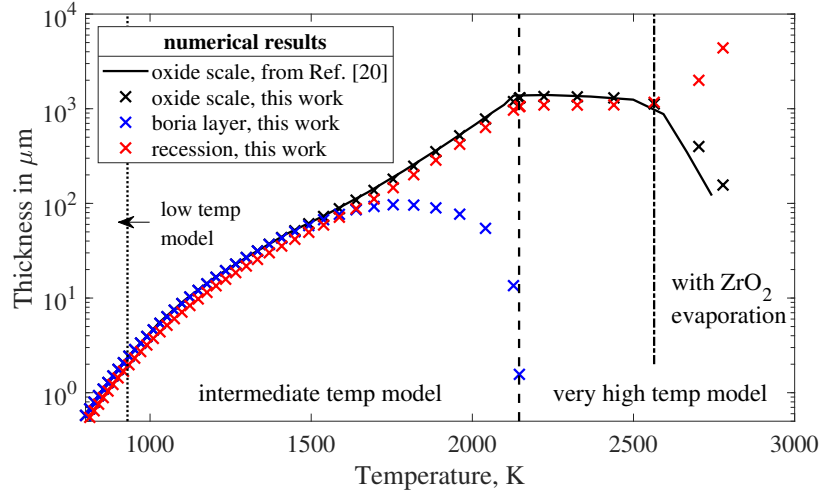


Fig. 10 Numerical model predictions for the oxide scale, recession and boron layer thickness after 1 hr exposure at 33 kPa of pure oxygen. Validation with the numerical prediction provided in Ref. [20].

One can see the distinguishing features of the temperature regimes. An external boron layer exists at low temperatures and evaporates at around 930 K, marking the transition from the low to intermediate temperature model. At approximately 2200 K, the internal boron layer between the oxide scale evaporates as well, activating the very high temperature model. This oxidation model contains a ZrO_2 evaporation term which becomes significant at around 2600 K.

The transition temperature of the oxidation models is also oxygen pressure dependent and will therefore vary with static pressure and oxygen mole fraction at the surface. This effect is illustrated in Fig. 11, which repeated the numerical calculations conducted for Fig. 10, but with different oxygen pressures.

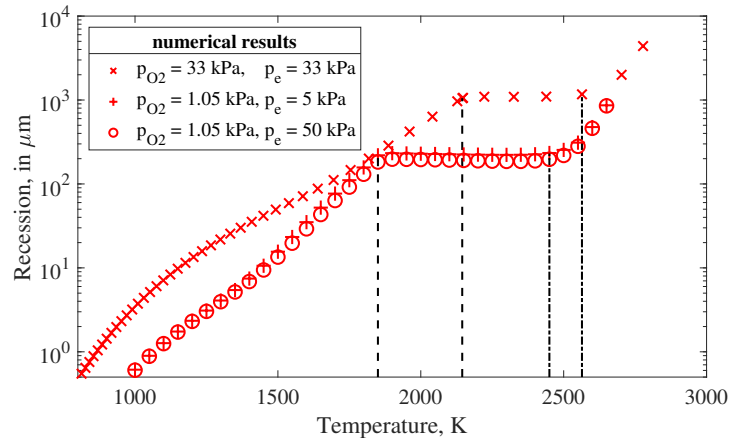


Fig. 11 Recession after 1 hour for different oxygen pressures.

At lower oxygen pressures, the transition temperature between the intermediate and the very high temperature

model is lower. This is due to a faster evaporation of the boria layer. The ZrO_2 evaporation is also enhanced and therefore occurs at lower temperatures. It is also interesting to note that the effect of oxygen pressure is largest in the very high temperature regime. In parts of the intermediate regime, at around 1800 K, the oxidation behavior appears to be completely independent of oxygen pressure. Minor differences persist due to the influence of the static pressure, p_e on empirically obtained quantities, such as the boria vapor mole fraction. Since the influence of p_e is small (Fig. 11), it is possible to visualize the oxidation behavior on a temperature - oxygen pressure map, shown in Fig. 12. The map shows the relative recession rate with respect to a reference case at 1 kPa oxygen pressure and 1375 K surface temperature. As expected, the recession rate increases with increasing temperature and decreasing oxygen pressure. The evaporation temperature for liquid boria and the oxide scale increases with increasing pressure.

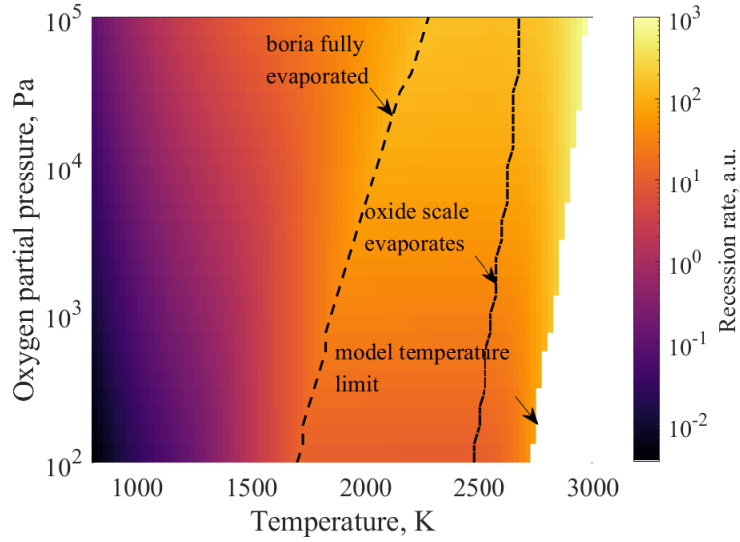


Fig. 12 Relative recession rate as a function of wall temperature and oxygen pressure.

Case B: Steady state flight case

A representative flight scenario, depicted in Fig. 13, is used to assess the potential of transpiration cooling on the oxidation behavior of real flight vehicles. Initially, a single trajectory point is investigated at the condition described in Table 3. This case has a cold wall heat flux of 7.1 MW/m^2 and includes mass injection. The thermophysical properties used to calculate the internal advective and conductive heat flux are summarized in Table 2.

Table 3 Overview of steady state flight condition.

Initial radius [mm]	Coolant [-]	B_h [-]	B^* [-]	\dot{m} [kg/m ² s]	Velocity [m/s]	Altitude [km]	$\dot{q}_{0,\text{cold}}$ [MW/m ²]	Flight time [s]
3	N ₂ , He	0 - 1.5	1.56, 0.6	0 - 1.66	3600	44	7.1	500

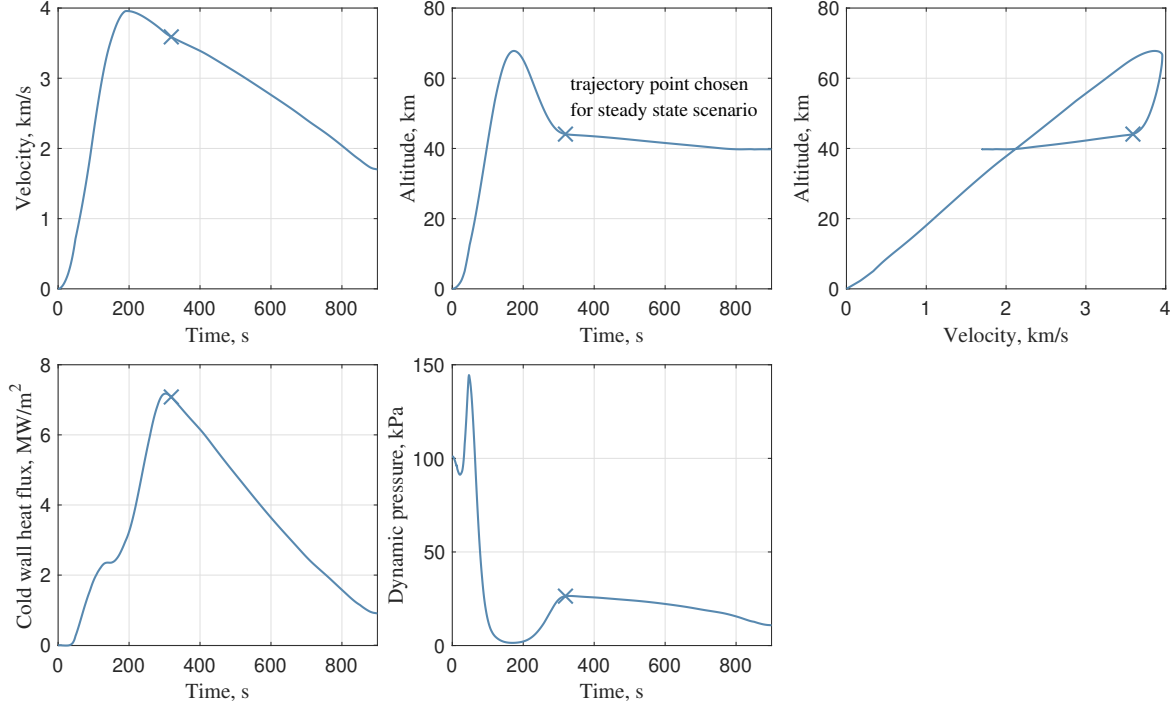


Fig. 13 Nominal trajectory of a hypersonic vehicle.

The initial radius, r_{t_0} , is provided for the start of the trajectory. Throughout the 500 second flight, the stagnation point will recess, blunting the nose. The heat flux and thus the surface temperature and the uncooled Stanton number, St_{h0} , were re-evaluated in time intervals of 1 second with an updated, effective radius. The 1-D model employed in this study cannot accurately model the 2-D deformation of the stagnation point. In order to obtain a first approximation of the blunting effect, the recession at every time step was added to the initial radius, to obtain the effective, blunted radius of curvature, as shown in Fig. 14.

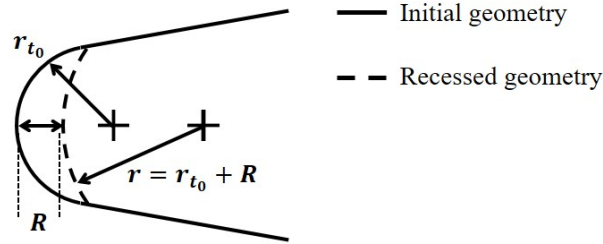


Fig. 14 Stagnation point blunting due to surface recession.

Figure 15 illustrates how transpiration cooling at different blowing parameters impacts the oxidation behavior. One can see that no blowing leads to 2.2 mm surface recession after 500 s flight at this condition. This amounts to 73% of the nose radius and will thus have significantly blunted the stagnation point. The dashed lines in Fig. 15 show what the heat flux and temperature would be if this blunting effect was ignored. The sharper radius would have increased

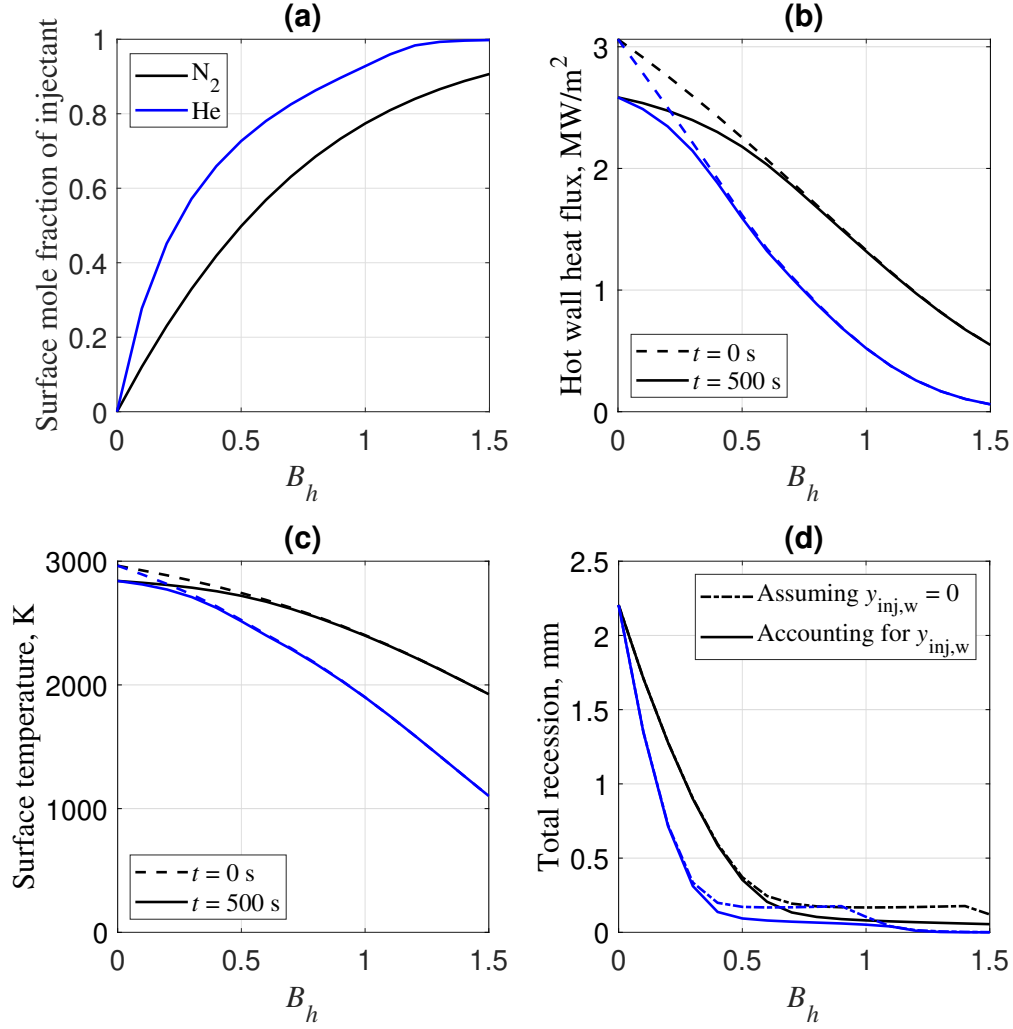


Fig. 15 Effect of blowing parameter on the wall quantities of a hypersonic stagnation point on a steady trajectory, as described in Table 3

the heat flux and thus the surface temperature. Fig. 16 shows the resulting increase in recession, in particular for the low blowing parameters. For no blowing, the recession would more than double. The dash-dotted line in Fig. 15 (d) highlights the importance of modelling the displacement of freestream oxygen by the injectant at the wall. If the oxygen displacement is ignored, and thus $y_{inj,w} = 0$, than the predicted recession is higher.

The geometry change caused by strong recession can lead to significant control problems and aerodynamic issues. It is caused by the elevated temperature of 2841 K that leads to the evaporation of ZrO_2 . This can be prevented by low to moderate blowing parameters.

Comparison of coolant gases

This section compares the injection of nitrogen and Helium gas. The comparison is made in two dimensions. Firstly, at a constant blowing parameter, for instance $B_h = 0.6$. Secondly, at the respective boundary layer blowoff parameter,

which is $B^* = 0.6$ for Helium and $B^* = 1.56$ for nitrogen.

For nitrogen, a blowing parameter of $B_h = 0.6$ reduces the surface recession to 0.21 mm. This is a significant improvement compared to the no blowing case. Nitrogen blowing ratios $B_h = 0.6 - 1.5$ are all in the very high temperature regime and therefore their oxidation protection is irrespective of temperature, as can be seen in Fig. 11. The improved oxidation protection provided by $B_h = 1.5$, compared to $B_h = 0.6$ is due to the higher surface mole fraction of the injected gas, reducing the partial pressure of freestream oxygen at the surface. The surface only recesses by 0.055 mm at $B_h = 1.5$. The effect of oxygen mole fraction is most pronounced at $B_h = 1.4$. The predicted surface recession, assuming that $y_{inj,w} = 0$ is 197% higher than when accounting for $y_{inj,w}$. This highlights the importance of modelling the concentration of oxygen on a hypersonic transpiration cooled stagnation point.

Helium generally outperforms nitrogen for the same blowing parameter. It is much more effective at displacing freestream air and reducing the surface temperature, as depicted in Fig. 15 (a) and (c). However, it is extremely light and thus for the same mass flux will have a much higher outflow velocity, which can disturb the external flow field. The boundary layer blowoff parameter (Eq. (7)) for Helium is just $B^* = 0.6$ and exceeding it is likely to cause injection induced turbulence and other secondary effects. Comparing both gases at their respective blowoff parameters, $B_h = 0.6$ for Helium and $B_h = 1.5$ for nitrogen, shows that nitrogen provides a slightly better oxidation protection. The total recession is 0.055 mm for nitrogen and 0.08 mm for Helium.

One cannot categorically say that one gas is superior to the other. Instead, it is highlighted that this comparison will depend on the metric. For the same B_h , Helium performs better. For the corresponding blowoff parameter, nitrogen performs better for this flight scenario. This currently ignores the greater system, where storage, weight and robustness must also be considered.

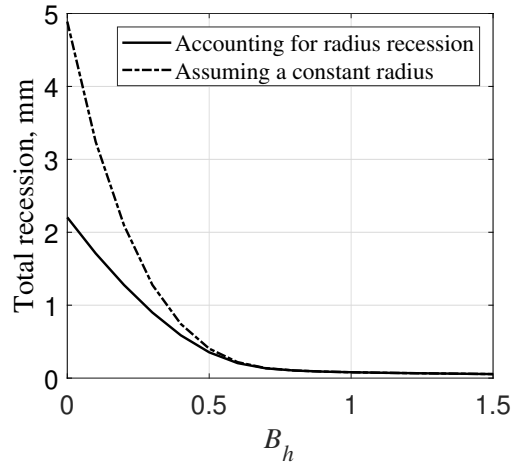


Fig. 16 Total radius recession after the 500 s steady state flight with nitrogen injection.

Case C: Transient flight path

The oxidation response of a transpiration cooled stagnation point is calculated for a nominal trajectory of a hypersonic vehicle, shown in Fig. 13. It was calculated using a quasi-steady time stepping method whereby the freestream conditions were assumed to be in steady state for 1 s before being updated. The surface recession and oxide scale thickness at the end of a quasi-steady time step were used as initial condition for the following time step.

The oxidation behavior is initially calculated with no mass injection, $B_h = 0$. Figure 17 (d) shows the surface recession over time. The oxidation starts at around 66 s, when the surface temperature exceeds 800 K and quickly enters the very high temperature regime at 112 s. At 250 s the evaporation temperature of ZrO_2 is exceeded, drastically reducing the oxide scale thickness. The oxide scale previously mitigated the diffusion of freestream oxygen to the surface. Removing it triggers a rapid acceleration in surface recession.

At approximately 300 s, the oxide scale starts growing again and thus the rate of recession decelerates. At 700 s, the surface temperatures falls below 2000 K, marking the transition into the intermediate oxidation regime. The oxide scale thickness plateaus at 0.15 mm. The total recession reaches 0.94 mm, which is equivalent to 31% of the 3 mm nose radius. The deformation of this key aerodynamic vehicle component is likely to lead to control problems and additional drag. Through mass injection at $B_h = 0.6$, the surface is kept up to 500 K cooler, as illustrated in Fig. 17 (c). The total surface recession in this cooled case only amounts to 0.13 mm or 4.3% of the radius. This is because the surface remains below the evaporation temperature of ZrO_2 , as depicted by the monotonically increasing red line in Fig. 17 (d).

Further increasing the blowing parameter to $B_h = 1.5$ moves a large proportion of the trajectory from the very high temperature into the intermediate temperature oxidation regime. This further reduces the recession thickness to 0.039 mm or 1.3% of the radius, due to the additional protection provided by the liquid boria layer.

Helium performs better for the same blowing parameter, as depicted in Fig. 17. The mole fraction of Helium at the wall is 78% and therefore higher than that of nitrogen at the same blowing parameter. Furthermore, Helium is much more efficient at reducing the incident heat flux and thus the wall temperature. The resulting recession at $B_h = 0.6$ is 0.075 mm and therefore 58% lower than that of nitrogen for the same B_h . If both coolants are compared at their boundary layer blowoff parameter, like in Case B, nitrogen outperforms Helium.

Fig. 17 (e) shows that the mass flux of nitrogen is only moderate for the blowing parameters considered, peaking at 1 kg/m²s and 2.5 kg/m²s, respectively. The same mass fluxes are required for Helium, as the blowing parameter and the freestream conditions are kept constant. The pressure required to drive a given mass flux through a porous medium is much higher for helium than for heavier gases, such as nitrogen. This might lead to structural problems or added mass for reinforced walls. A full systems study, taking into account the vehicle mass is thus required to assess which coolant is more suited for a specific mission and vehicle type. The analysis shown in this paper will provide the coolant mass needed to achieve a certain oxidation protection and can be used to optimise the performance of this subsystem.

One can see that much mass flux is injected in the first 66 s, during which no oxidation occurs for the no injection

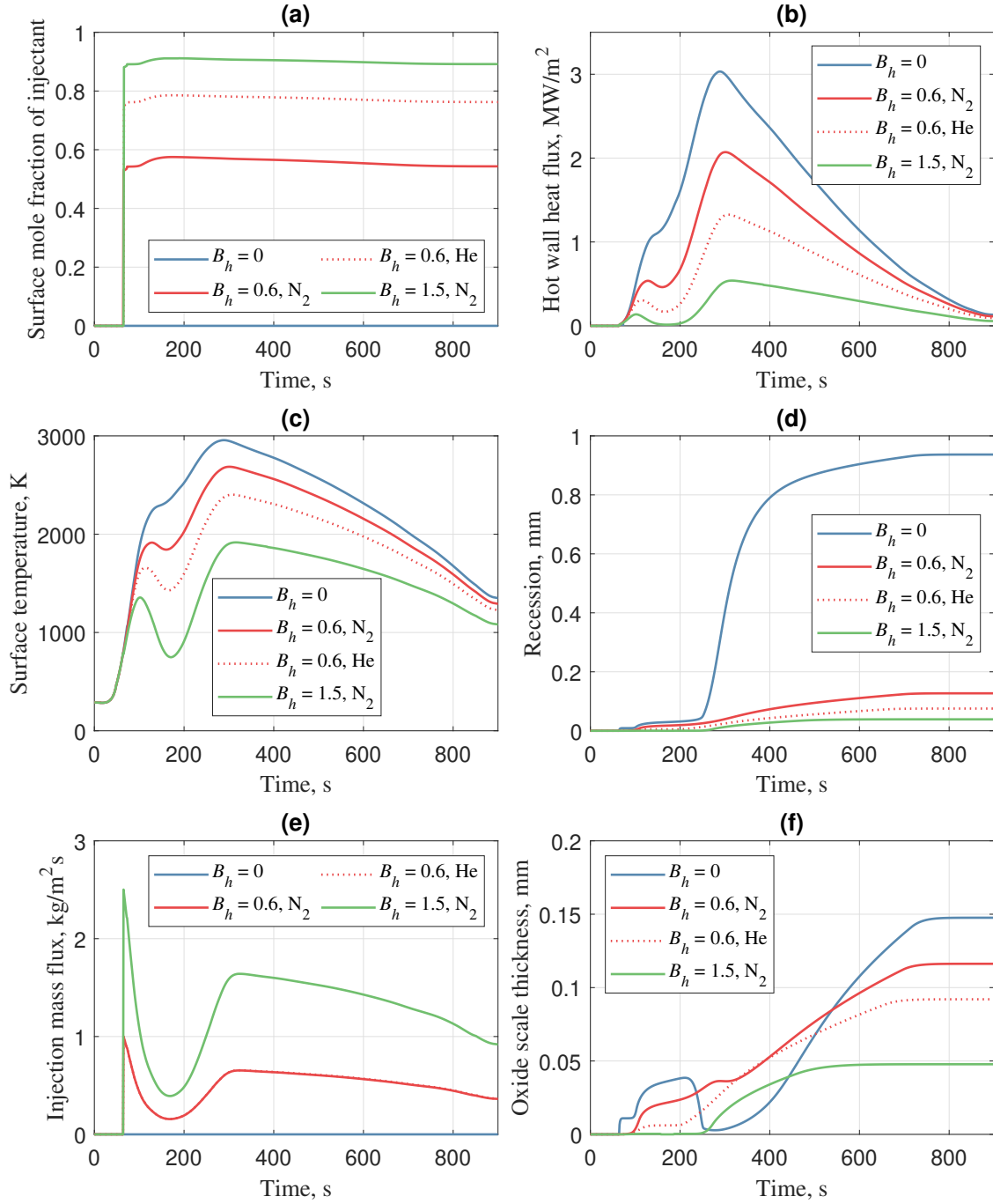


Fig. 17 Material response injection properties of the transpiration cooled stagnation point.

case. To reduce system mass, it is desirable to only inject gas when it is really needed. Constant blowing parameters throughout the transient trajectory are not optimal. Instead, a real system would adjust the blowing parameter such that the ZrO_2 evaporation regime is never entered.

It is important to note that several real-flight phenomena were not accounted for in this analysis. The employed oxidation model has only been validated experimentally in the furnace. The hypersonic flow is likely to enhance the evaporation of the boron layer and the oxide scale. Vibration, shear and pressure forces may cause the oxide layer to spall. The comparison with transpiration experiments was attempted in Ref. [8], but only provided qualitative results due to large uncertainties. A second experiment will be undertaken soon. First encouraging results were obtained in Ref. [12] for a similar material. A UHTC, specifically 20 vol%SiC-HfB₂, was exposed to simulated hypersonic flight conditions. The corresponding oxidation model predicted the recession within reasonable error, showing that the above mentioned effects were only secondary.

Further, questions on the practical implementation of this system remain. Ref. [9] has shown that porous ZrB₂ at pore sizes of less than 10 μm is manufacturable, resulting in a high flow uniformity, coupled with good structural strength. Further work is required to make a more complex cooling architecture. The practical implementation will also hinge on the weight penalty incurred by the coolant gas, pressure tanks, valves and other system components. Together with added safety layers and redundancy due to the high system complexity of transpiration cooling the disadvantages might outweigh the benefits of this cooling technology. Future work to quantify these effects is encouraged.

IV. Conclusion

This paper presents the methodology and results of a systems study on the material response of transpiration cooled hypersonic stagnation points. A validated oxidation model for ZrB₂ was used to compute the recession and oxide scale thickness. A recently developed correlation for a hypersonic stagnation point with blowing provided the oxygen partial pressure at any flight condition, which is a critical input parameter for the oxidation model. The surface temperature was computed using validated low-order models, which take into account the heat flux reduction due to the coolant film.

A representative steady state flight scenario at 44 km altitude and 3.6 km/s velocity is chosen to assess the effect of mass injection on the oxidation behavior. No blowing causes the 3 mm radius to recess by 73%. Moderate amounts of blowing ($B_h = 0.6$) reduce this recession to just 4.3%. The displacement of freestream air at the surface through transpiration cooling has a strong effect on the oxidation behavior. If it is not accounted for, the recession increases by as much as 197%.

The total surface recession along the transient flight path of an envisaged hypersonic vehicle with a 3 mm nose radius exceeds 0.93 mm. This could lead to aerodynamic and control problems. With a moderate blowing parameter of $B_h = 0.6$, the recession can be reduced to 0.13 mm and 0.075 mm, for N₂ and He injection, respectively. The required mass flux does not exceed 1 kg/m²s.

Funding Sources

This research is funded by the EPSRC grant "Transpiration Cooling Systems for Jet Engine Turbines and Hypersonic Flight" (reference: EP/P000878/1).

Acknowledgments

The authors would like to thank Hassan Saad Ifti and Imran Naved for their helpful comments.

References

- [1] Heppenheimer, T. A., *Facing the heat barrier: a history of hypersonics*, Vol. 4232, Government Printing Office, 2009.
- [2] Hermann, T., McGilvray, M., and Naved, I., "Performance of Transpiration-Cooled Heat Shields for Reentry Vehicles," *AIAA Journal*, Vol. 58, No. 2, 2020, pp. 830–841. <https://doi.org/10.2514/1.J058515>.
- [3] Loehman, R., Corral, E., Dumm, H. P., Kotula, P., Tandon, R., et al., "Ultrahigh-Temperature Ceramics For Hypersonic Vehicle Applications," *Industrial Heating*, Vol. 71, No. 1, 2004, pp. 36–38. <https://doi.org/10.2172/887260>.
- [4] Francese, A., "Numerical and experimental study of UHTC materials for atmospheric re-entry," *Dottorato di ricerca in ingegneria aerospaziale*, 2007.
- [5] Reimer, T., Kuhn, M., Gülhan, A., Esser, B., Sippel, M., and van Foreest, A., "Transpiration cooling tests of porous CMC in hypersonic flow," *17th AIAA International Space Planes and Hypersonic Systems and Technologies Conference*, 2011, p. 2251. <https://doi.org/10.2514/6.2011-2251>.
- [6] Bacos, M., "Carbon-carbon composites: oxidation behavior and coatings protection," *Le Journal de Physique IV*, Vol. 3, No. C7, 1993, pp. C7–1895. <https://doi.org/10.1051/jp4:19937303>.
- [7] Parthasarathy, T., Rapp, R., Opeka, M., and Kerans, R., "A model for the oxidation of ZrB₂, HfB₂ and TiB₂," *Acta Materialia*, Vol. 55, No. 17, 2007, pp. 5999–6010. <https://doi.org/10.1016/j.actamat.2007.07.027>.
- [8] Ewenz Rocher, M., McGilvray, M., Hermann, T. A., Ifti, H. S., Hufgard, F., Eberhart, M. F., Meindl, A., Loehle, S., Giovannini, T., and Vandeperre, L. J., "Testing a transpiration cooled zirconium-di-boride sample in the plasma tunnel at IRS," *AIAA Scitech 2019 Forum*, 2019, p. 1552. <https://doi.org/10.2514/6.2019-1552>.
- [9] Ifti, H. S., Hermann, T., McGilvray, M., Larrimbe, L., Hedgecock, R., and Vandeperre, L., "Flow Characterization of Porous Ultra-High-Temperature Ceramics for Transpiration Cooling," *AIAA Journal*, 2022, pp. 1–12.
- [10] Otsu, H., Fujita, K., and Ito, T., "Application of the transpiration cooling method for reentry vehicles," *45th AIAA Aerospace Sciences Meeting and Exhibit*, 2007, p. 1209. <https://doi.org/10.2514/6.2007-1209>.
- [11] Ewenz Rocher, M., Hermann, T., McGilvray, M., Grossman, M., and Vandeperre, L., "Measuring the concentration of freestream species on a hypersonic transpiration cooled stagnation point," 2021.

- [12] Parthasarathy, T. A., Petry, M. D., Cinibulk, M. K., Mathur, T., and Gruber, M. R., “Thermal and oxidation response of UHTC leading edge samples exposed to simulated hypersonic flight conditions,” *Journal of the American Ceramic Society*, Vol. 96, No. 3, 2013, pp. 907–915. <https://doi.org/10.1111/jace.12180>.
- [13] Naved, I., Hermann, T., and McGilvray, M., “Numerical Simulation of Transpiration Cooling for a High-Speed Vehicle with Substructure,” *AIAA Journal*, 2021, pp. 1–12. <https://doi.org/10.2514/1.J059771>.
- [14] Fay, J. A., and Riddell, F. R., “Theory of stagnation point heat transfer in dissociated air,” *Journal of the Aerospace Sciences*, Vol. 25, No. 2, 1958, pp. 73–85. <https://doi.org/10.2514/8.7517>.
- [15] Yoshikawa, K. K., *Linearized theory of stagnation point heat and mass transfer at hypersonic speeds*, Vol. 5246, National Aeronautics and Space Administration, 1969.
- [16] Schweikert, S., von Wolfersdorf, J., Selzer, M., and Hald, H., “Characterization of actively cooled porous C/C wall segments according to pressure loss and internal temperature distribution,” *7th European Workshop on Thermal Protection Systems & Hot Structures*, ESA Conference Bureau Noordwijk, The Netherlands, 2013.
- [17] Ewenz Rocher, M., Hermann, T., McGilvray, M., and Gollan, R., “Correlation for Species Concentration on a Hypersonic Stagnation Point with Mass Injection,” *AIAA Journal*, 2021, pp. 1–12.
- [18] Snyder, C., “CEARUN,” , 2012. <https://cearun.grc.nasa.gov>.
- [19] Bird, R. B., “Transport phenomena,” *Appl. Mech. Rev.*, Vol. 55, No. 1, 2002, pp. R1–R4.
- [20] Parthasarathy, T., Rapp, R. A., Opeka, M., and Kerans, R. J., “A model for transitions in oxidation regimes of ZrB₂,” *Materials Science Forum*, Vol. 595, Trans Tech Publ, 2008, pp. 823–832. <https://doi.org/10.4028/www.scientific.net/MSF.595-598.823>.